Submitted to Acta Materialia (August 2017)

Using heat treatments, high-pressure torsion and post-deformation annealing to optimize the properties of Ti-6Al-4V alloys

Hamed Shahmir, Terence G. Langdon*

Materials Research Group, Faculty of Engineering and the Environment,
University of Southampton, Southampton SO17 1BJ, UK

Abstract

Experiments were conducted to investigate the processing parameters that may be used to optimize the properties of Ti-6Al-4V alloys. The alloy was initially subjected to two different heat treatments leading to the formation of martensitic α′ and lamellar α+β microstructures and then both materials were processed by high-pressure torsion (HPT) for 10 turns at room temperature. This gave significant grain refinement to the nanometer range in both conditions and the occurrence of an allotropic *hcp* to *fcc* phase transformation in the martensitic alloy. These nanostructured alloys were subjected to post-deformation annealing (PDA) at temperatures in the range of 473 to 1023 K. The results show the hardness increases slightly to 773 K due to $\alpha'+fcc\rightarrow\alpha+\beta+fcc$ and $\alpha\rightarrow\alpha+\beta$ phase transformations in the martensitic α′ and lamellar α+β alloys and then decreases up to 1023 K due to recrystallization and grain growth. An optimum property of a very high yield strength (~1120 MPa) and ultimate tensile strength (~1200 MPa), together with excellent ductility (elongation to failure of ~26%), was achieved in the Ti-6Al-4V martensitic alloy processed by a combination of HPT followed by PDA at 873 K for 60 min.

Keywords: High-pressure torsion; Nanostructured materials; Phase transformations; Post-deformation annealing; Ti-6Al-4V alloy.

*Corresponding author: e-mail address: langdon@soton.ac.uk

1. Introduction

Ti-6Al-4V is the titanium alloy used most frequently in commercial and industrial applications. This alloy possesses low density, high strength, good toughness, a general corrosion resistance, excellent bio-compatibility and very good high temperature properties and formability. Therefore, it is used widely for many applications in aerospace and chemical engineering, for power generation and as an implant material in medicine [1-4]. In equilibrium, the alloy consists mainly of an α-phase (*hcp*) with some β-phase (*bcc*) at room temperature. The existence of the α/β transformation means that it is possible to achieve a variety of microstructures and property combinations in the alloy through thermo-mechanical processing thereby permitting the development of properties for specific applications [5].

Depending upon the cooling rate and the prior heat treatment, the microstructure of the alloy may be divided into several types. For very slow cooling rates from high within the α+β region or above the β-transus temperature (1263 ± 20 K), the β-phase primarily transforms into a globular type of α. Increasing the cooling rate accelerates the α nucleation rate in the β grain boundaries thereby enhancing the formation and growth of α platelets into prior β grains. The β-phase fully or partly transforms into a martensitic type during high cooling rates and this martensite exists in two different forms, α′ (*hcp*) and α" (orthorhombic) [6-8]. The type and amount of α′ and α" formed on quenching depends upon the chemical composition (vanadium enrichment) of the β phase that exists at the temperature prior to quenching [9]. Thus, by controlling the phase transformations occurring during thermal processing, particularly during cooling from elevated temperatures, an optimal mechanical performance may be achieved in the α+β Ti alloys.

It is now well established that grain refining is a very effective procedure for improving the mechanical properties of materials. Furthermore, processing through the application of severe plastic deformation (SPD) provides an opportunity for reducing the grain size to the submicrometer or even the nanometer level [10,11]. In practice, high-pressure torsion (HPT) is an excellent processing method because it produces materials with exceptionally small grain sizes and with a large fraction of grain boundaries having high angles of misorientation [12-14]. In HPT a disk-shaped specimen is deformed by simple shear between two anvils where it is constrained under a high pressure and subjected to concurrent torsional straining [15]. Generally, nanostructured metals and alloys processed by HPT exhibit high strength but their ductility is limited because they have both a low rate of strain hardening and a low strain rate sensitivity [16-18]. Accordingly, post-deformation annealing (PDA) is often an important tool for improving the ductility both for titanium [19] and for other materials [20,21]. Nevertheless, annealing at excessively high temperatures may lead to an acceleration in recovery and a reduction in hardness so that it is important to select an appropriate annealing condition to produce both good ductility and high strength [22].

Several reports are now available describing the processing of the Ti-6Al-4V alloy by HPT [23-29] but no systematic investigations are available describing the effect of the initial microstructure on the structural evolution and on the mechanical behavior of the alloy after PDA. Furthermore, there has been no attempt to date to optimize the properties of Ti-6Al-4V alloys using selected combinations of HPT and PDA. Accordingly, the present investigation was initiated to address this deficiency by subjecting a Ti-6Al-4V alloy to two different heat treatments in order to produce significantly different initial microstructures and then evaluating the significance of these initial conditions on the subsequent microstructural evolution and the mechanical properties attained within the alloy after HPT and PDA.

2. Experimental material and procedures

The experiments were conducted using a Ti-6Al-4V alloy where the composition is given in wt%. Prior to processing by HPT, the as-recieved material was divided into two separate batches and these batches were treated using two different heat treatments. The first batch was subjected to a solution annealing at 1273 K for 30 min followed by water quenching to obtain a martensitic microstructure. The second batch was solution annealed at 1223 K for 45 min followed by air cooling to room temperature and then a stress relief anneal at 873 K for 3 h followed by furnace cooling to obtain a lamellar (α+β) microstructure. Henceforth, the materials processed by these two procedures are denoted as α′ (martensitic) and α+β (lamellar), respectively. Following the initial heat treatments, disks with thicknesses of ~0.8 mm and diameters of 10 mm were processed by HPT at room temperature under an applied pressure of P = 6.0 GPa using a rotation speed of 1 rpm and rotations through totals of 10 revolutions under quasi-constrained conditions [30]. These disks were then processed by PDA at temperatures from 473 to 1023 K for 60 min.

Each processed disk was polished to a mirror-like quality and hardness measurements were taken using a Vickers microhardness tester with a load of 500 gf and a dwell time of 10 s. The average microhardness values, Hv, were measured at 3 mm from the disk centres and at every point the local value of Hv was obtained from an average of five separate hardness measurements. The phase constituents were determined using X-ray diffraction (XRD) employing Cu Kα radiation (wavelength λ = 0.154 nm) at 45 kV with a tube current of 200 mA. The XRD measurements were performed over a 2θ range from 30° to 90° using a scanning step of 0.01° and a scanning speed of 2° min^{-1}. The analysis using XRD was conducted over sample areas with diameters of 3 mm located near the edges of the disks. Microstructural characterizations were carried out using optical microscopy (OM), scanning electron microscopy (SEM) and transmission electron microscopy (TEM). Foils for TEM were prepared after HPT processing using a focused ion beam (FIB) Zeiss Nvision 40 FIB facility at 3 mm from the disk centres in the normal sections of the disks so that the normals of the images lay in the shear direction. The TEM micrographs were obtained using a JEOL JEM-3010 microscope operating under an accelerating voltage of 300 kV.

Two miniature tensile specimens with gauge dimensions of 1.1 × 1.0 × 0.6 mm^3 were cut from symmetric off-centre positions near the edges of each disk using electro-discharge machining. The mechanical properties were examined in the martensitic and lamellar alloys after HPT followed by PDA at 773 to 1023 K for 60 min. Stress-strain curves were recorded using an initial strain rate of 1.0×10^{-3} s^{-1} with a Zwick universal testing machine. Two samples were tested for each condition. The stress-strain curves were plotted for each specimen and the ultimate tensile strengths were derived directly from the curves. The elongations were also estimated by carefully measuring the gauge lengths before and after tensile testing using an optical microscope.

3. Experimental results

3.1 Microstructures of the Ti-6Al-4V alloy before and after HPT processing

The microstructure of the alloy after solution annealing at 1273 K for 30 min followed by water quenching is shown in Fig. 1(a). The coarse prior β grains, with an average size of ~500 μm, were fully transformed to martensite (α′) and the microstructure shows martensitic laths distributed throughout the microstructure having different orientations and with an average lath thickness of ~0.8 μm. Figure 1(b) shows the microstructure after solution annealing at 1223 K for 45 min followed by air cooling to room temperature and then stress relief annealing at 873 K for 3 h followed by furnace cooling. The microstructure reveals a lamellar α+β structure having different orientations. In the lamellar α+β the retained β-phase lies between the α platelets so that the resulting microstructure consists of average prior-β grains of ~500 μm, colony size parallel-oriented α-phase lamellae of ~200 μm and an average α lamellae lath width of ~1.5 μm.

TEM micrographs and selected area electron diffraction (SAED) patterns of the HPT processed α′ and α+β alloys are shown in Fig. 2(a) and (b), respectively, taken at regions of ~3 mm from the disk centres. The microstructures of both conditions are highly strained from the HPT processing with complex non-uniform contrasts because of the presence of high densities of lattice defects. These images show that many grains have an irregular shape with sharp corners while many of the grain boundaries are wavy and ill-defined. Some equiaxed grains appear to form from the fragmentation of elongated grains and these and other similar images suggest that the average sizes of the separate fragments of structures are ~30 and ~40 nm for the processed α′ and α+β alloys, respectively. The diffraction patterns show numerous spots arranged along circles indicating the presence of crystallites separated by high-angle grain boundaries (HAGBs). The appearance of significant streaking of the diffraction spots denotes the presence of high internal stresses and elastic distortions of the crystal lattice. All of these characteristics are typical of materials prepared using SPD techniques and they are consistent with the presence of a large volume of high-energy non-equilibrium grain boundaries [31-34]. The observed diffraction patterns correspond to the α/α′-phase and the *fcc* phase for the processed α′ samples but only to the α-phase for the processed α+β samples. Thus, in the latter material there is no evidence for the presence of a β-phase and this demonstrates the dissolution of the β-phase during the SPD-processing.

Further observations of the microstructure of the HPT-processed α′ alloy by TEM and the relevant SAED pattern are given in Fig. 3(a). The dark-field image in Fig. 3(b) is based on the spot corresponding to the *fcc* phase marked by a circle in the diffraction pattern in Fig. 3(a) and it shows the distribution of this phase within the *hcp*-phase matrix and suggests the occurrence of twinning in *fcc*.

3.2 Mechanical properties after PDA

Figure 4 shows the measured values of the microhardness for the HPT-processed samples before and after annealing at temperatures from 473 to 1023 K for a period of 60 min. The lower dashed lines in Fig. 4 correspond to the initial hardness values before HPT processing of ~330 and ~290 for the α′ and α+β alloys, respectively, thereby demonstrating that the hardness of the martensitic alloy is initially significantly higher than the lamellar alloy. Inspection of Fig. 4 shows that, with reference to the initial conditions, the hardness near the edges of the α′ and α+β disks increases after 10 turns to ~390 and ~350, respectively. The results show that the hardness of the nanocrystalline α′ and α+β alloys increases slightly up to ~410 and ~395, respectively, after annealing at 773 K and then decreases rapidly with increasing annealing temperatures up to 1023 K. At this latter temperature, the hardness is close to the value for the initial α+β alloy.

Representative plots of engineering stress against engineering strain are shown in Fig. 5 using an initial strain rate of 1.0×10^{-3} s^{-1} for initial conditions for (a) α′ and (b) α+β samples and after PDA for 60 min at temperatures from 773 to 1023 K. Table 1 provides a comprehensive summary of the mechanical properties data derived from the various samples including the hardness, Hv, the yield stress (YS), the ultimate tensile strength (UTS) and the elongation to failure, δ%.

Figure 5(a) shows results for the initial martensitic sample with high UTS of ~1190 MPa and an elongation to failure of ~20% with a flow curve exhibiting strain hardening. Annealing of the α′ HPT-processed sample at 773 K gives a reasonable UTS of ~1250 MPa that is a direct consequence of the HPT processing but there is only a very limited elongation of ~1% and without any strain hardening. The elongations to failure of samples subjected to PDA above 873 K reveal a significant improvement but with corresponding reductions in the UTS. Thus, PDA at temperatures of 873 and 923 K appear to give reasonable strength coupled with a good ductility. The results show the strength decreases and the elongation to failure increases with increasing annealing temperature up to 973 K but with a reduction in the elongation at 1023 K. From these results it is concluded that PDA at 873 K for 60 min leads to excellent mechanical properties with a UTS of ~1200 MPa and an elongation of ~26%.

Representative plots of engineering stress against engineering strain are shown in Fig. 4(b) for the α+β alloy where the initial lamellar sample shows significant strain hardening with a low UTS of ~730 MPa and an elongation to failure of ~23%. Nevertheless, it is apparent that HPT through 10 turns followed by PDA leads to a very significant improvement in the mechanical properties with a maximum UTS of ~1180 MPa and an elongation of ~15% in the α+β alloy after PDA at 873 K for 60 min. Inspection of all curves shows that the strength decreases and the elongation increases with increasing annealing temperature except at the highest temperature of 1023 K where, similar to the martensitic alloy, there is a slight decrease in the elongation to failure.

3.3 Microstructure after PDA

Figure 6 shows the X-ray diffraction patterns of (a) the α′ and (b) the α+β alloys in the initial condition, after HPT through 10 turns and after HPT + PDA at 773, 873 and 973 K at the edge areas of the disks. As anticipated, the microstructure of the martensitic alloy consists only of martensite with a main peak of $(101)_{\alpha/\alpha'}$ (Fig. 6(a)). This is consistent with an earlier report in which a high solution heat treatment temperature (>1173 K) led to a lower vanadium enrichment in the β phase and thus to a transformation into α′ instead of α" upon quenching [35]. However, the microstructure of the lamellar alloy in Fig. 6(b) shows α-phase peaks with a main peak of $(101)_{\alpha/\alpha'}$ and a peak corresponding to the $(110)_{\beta}$ plane at $2\theta \approx 39.6°$ confirming the existence of the β-phase in the microstructure. The volume fraction of β-phase at the latter heat-treated condition was only ~6% calculated using standard procedures [36].

The XRD patterns of the martensitic alloy show clearly the appearance of new peaks after HPT processing (Fig. 6(a)) at $2\theta = 44.5°$ and $2\theta = 64.4°$ marked with open inverted triangles and this corresponds to the (200) and (220) planes of the *fcc* structure. The volume fraction of the *fcc* phase was estimated as ~40% after HPT through 10 turns. Nevertheless, for the α+β alloy there was no evidence for *fcc* or β phases in the X-ray diffraction patterns. Therefore, since the initial condition of this alloy consisted of α and β phases, these results confirm the dissolution of the β-phase during HPT which is consistent with earlier results [37].

Comprehensive evaluations of the nanostructured Ti-6Al-4V alloys during PDA showed that the microstructures exhibited no significant change after annealing at 773 K except for a reduction in the peak broadening. Nevertheless, the peak corresponding to the $(110)_{\beta}$ plane at $2\theta \approx 39.6°$ appeared after annealing at temperatures of 873 and 973 K. Close inspection of Fig. 6(a) reveals that the *fcc*-phase is stable after PDA up to 973 K but the intensity of this phase decreases significantly.

A set of representative SEM images is presented in Fig. 7 for the α′ and α+β alloys after PDA at 923, 973 and 1023 K for 60 min. These images show that the microstructures of the samples consist of equiaxed fine grains after PDA and, as marked, there are some grains with lamellar α+β microstructures surrounded by α grains. The results demonstrate clearly that the grain size increases with increasing PDA temperature in both alloys and the average grain sizes in the α+β alloy are larger than in the α′ alloy. Measurements gave average grain sizes in the α′ alloy of ~0.6, ~0.8 and ~1.5 μm after PDA at 923, 973 and 1023 K, respectively. The corresponding values for the α+β alloy were ~1.0, ~1.2 and ~3.0 μm after PDA at the same three temperatures.

4. Discussion

4.1. Microstructural evolution during HPT processing

Using appropriate heat treatments, two different initial microstructures of the Ti-6Al-4V alloy were subjected to HPT for 10 turns and the results show the development of different hardnesses and significant different microstructures after processing. The hardness of the α′ alloy is higher (Hv ≈ 390) and the grain size is smaller (~30 nm) than for the α+β alloy (Hv ≈ 350 and grain size of ~40 nm). The initial martensitic phase with a high level of residual stress has a substructure containing predominately dislocations and stacking faults with a few platelets containing twins due to the shear transformation and a supersaturated chemical composition [38] and this explains the microstructural difference between the two alloys after HPT. In general, an investigation of the initial conditions shows that the volume fractions of boundaries in the α′ and α+β structures are high but not as high as in the α′ alloy. These boundaries act as nucleation sites for grain fragmentation together with subgrain formation during the initial stages of deformation.

It is important to note that the initial crystal structure of the martensitic alloy is *hcp* and, based on the low volume fraction of the β (*bcc*) phase in the α+β alloy (only 6%), it is reasonable to assume that the *hcp*-α phase controls the deformation mechanism in both alloys.

Twinning plays an important role in the deformation mechanism of coarse-grained *hcp*-Ti due to the lack of a sufficient number of slip systems and twining undoubtedly plays a significant role in grain refinement at least in the early stages of deformation [39-42]. In fact, the introduction of extra interfaces within the grains during deformation twinning leads to significant grain refinement and extraordinary increments in hardness during HPT processing at room temperature including during the further straining following the saturation of twinning. It was reported that, after large amounts of plastic deformation, the twins break up into subcells and also the twinning propensity decreases with decreasing grain size in Ti during SPD processing [40]. Therefore, a new deformation mechanism is needed to accommodate this flow. The present results suggest that the *hcp* to *fcc* phase transformation plays an important role in the accommodation of constrained deformation in the highly-defect martensitic alloy. The α′ (*hcp*) alloy consists of a high volume fraction of boundaries and the substructure contains predominately dislocations and stacking faults with a few platelets containing twins: therefore, this microstructure leads to significant grain refinement and these defects promote the formation of an *fcc* phase during HPT processing [43].

4.2. Microstructural evolution during PDA

The results from these experiments show clearly that the single α′-phase changes to a dual α′+*fcc*-phase and the dual α+*β*-phase changes to a single α-phase after HPT processing through 10 turns. Nevertheless, the results show further that the heavily deformed α′ and α transform to equilibrium α and β during PDA so that α′+*fcc*→*α*+*β*+*fcc* and α→*α*+*β* phase transformations occur in the former and latter conditions, respectively. Close inspection of the hardness data shows that the hardness increases slightly up to 773 K due to the formation of the new phase and thereafter decreases to 1023 K due to a combination of recrystallization and grain growth. The hardness evolution with annealing temperatures in Fig. 4 suggests that the onset of decomposition occurs at 573 K but the β-phase is detectable after annealing at 873 K according to the XRD results in Fig. 6. The SEM images show clearly some equiaxed grains containing lamellar α+β structure after PDA at 923 K and this confirms the occurrence of recrystallization at this temperature in both alloys. The results also demonstrate that the grains remain very fine even after annealing at 1023 K for 60 min.

It was suggested earlier that the fine precipitation of α and β phases from the fully martensitic structure occurs by a nucleation and growth process controlled by atomic diffusion at the martensite plate boundaries or at internal structures such as twins [44]. The volume fraction of the β-phase in both alloys increases by increasing the annealing temperature, but the present investigation shows there is a very low volume fraction of the β-phase in the HPT-processed Ti-6Al-4V alloy for the two initial conditions after PDA (less than 5%). These results demonstrate that the *fcc*-phase decreases by increasing the annealing temperature in the α′ alloy and this phase is stable even after annealing at 973 K. It was reported earlier that the *fcc*-phase, which was detected after a solid solution treatment and subsequent water quenching in a Ti-20Zr-6.5Al-4V alloy, completely decomposed into an α-phase after annealing at 973 K [45].

4.3. Mechanical properties after PDA

Despite the success in achieving a highly-refined microstructure in the Ti-6Al-4V alloy, it is reasonable to anticipate that the tensile properties of the nanostructured Ti-6Al-4V specimens processed by HPT are not satisfactory when testing at room temperature. It is readily apparent from Fig. 5(a) that the tensile properties after HPT and PDA at 773 K show a very limited elongation to failure due directly to the HPT processing. Accordingly, an optimization of these properties requires PDA of the nanostructured specimens under appropriate conditions in order to improve the ductility. The present investigation shows that it is possible to achieve a very high yield strength (~1120 MPa) and UTS (~1200 MPa) in addition to good ductility (elongation to failure of ~26%) through a combination of HPT processing of the initial martensitic state and PDA at 873 K for 60 min. Specifically, PDA below 973 K is beneficial because it improves the ductility without significantly decreasing the strength whereas PDA at

973 K and higher leads to an acceleration in recovery and grain growth and thereby leads to a strength reduction.

The results show clearly the effect of the initial microstructure on the mechanical properties of samples after HPT processing followed by PDA. Thus, the initial martensitic microstructure leads to greater grain refinement during HPT processing and the average of grain sizes of samples are smaller after PDA. This additional grain refinement is directly responsible for the improved mechanical properties of the martensitic alloy.

There are also other important difference in the two alloys relating to the existence of the *fcc*-phase in the martensitic alloy after PDA. It can be deduced from these experiments that the *fcc*-phase improves the material strength and this is consistent with results on the Ti-20Zr-6.5Al-4V alloy [45]. Thus, it appears that the easy gliding basal $\langle a \rangle$ slip in the matrix is effectively blocked at the phase interface due to the discontinuity of slip across the interface and this is confirmed by a recent report in which the room-temperature yield strength of polycrystalline Ti was observed to increase from ~381 to ~731 MPa after formation of the *fcc*-phase [46].

All of these results show that the β-phase may affect the measured elongations to failure. The initial lamellar microstructure shows lower elongations to failure by comparison with the martensitic alloy after PDA at 873 to 1023 K and the lamellar alloy after PDA at 973 and 1023 K. The XRD results show clearly that the volume fraction of the β-phase in the initial lamellar microstructure is a maximum at ~6%. In addition, the results demonstrate that the volume fraction of this phase is increased by increasing the annealing temperature and this explains the lower elongation to failure of samples after PDA at 1023 K by comparison with PDA at 973 K.

4.4 Significance of using miniature configurations in the testing of HPT samples

It is important to note that the results obtained in tensile testing are dependent not only upon the properties of the material and the testing conditions, including the strain rate and temperature, but also upon the specimen size and geometry. For example, experiments have shown that the measured elongations to failure in tensile testing tend to increase with decreasing gauge length [47,48] and this is because the area of necking constitutes a major fraction of the gauge length in samples with very short gauge lengths so that much of the measured elongation in simple tensile testing is related to flow in the necked region. This suggests, therefore, that it may be unreasonable to make a direct comparison between the total elongations achieved in conventional tensile testing with longer gauge lengths with the results obtained in tensile testing using HPT samples with gauge lengths only of the order of ~1 mm. Instead, it appears initially that more realistic data may be obtained by measuring the uniform strain that occurs prior to the formation of the neck.

Despite these apparent difficulties associated specifically with miniature samples, the use of miniature tensile specimens cut from the 10 mm disks that are prevalent in conventional HPT processing is now becoming a standard testing procedure. Therefore, the present experiments provide important data on the total elongations to failure and these results may be compared directly with the data obtained in many other similar investigations. Furthermore, it is important to note that the gauge thicknesses in the HPT tensile samples are very small, typically of the order of ~0.6 mm, and it is found in practice that this leads to premature failure because there are insufficient grains in the cross-sectional areas to maintain deformation to very high elongations. As a result, experiments have shown that the tensile elongations recorded with HPT samples are generally smaller, not larger, than the elongations attained with conventional tensile samples. For example, this was demonstrated in a very recent report comparing the elongations to failure achieved in samples prepared by different processing procedures, including HPT, in various Al-Mg-Sc alloys [49]. It should be noted also that, whereas an increase in the measured total elongation was reported for a Ti-6Al-4V alloy sheet using conventional cross-sections but gauge lengths smaller than 10 mm, there was no significant effect of gauge length on the strength characteristics including both the YS and the

UTS [50]. Based on this information, it is therefore concluded that the present results, with a very high yield strength of ~1120 MPa and an elongation to failure of ~26%, provide a reasonable description of the Ti-6Al-4V alloy under the specific conditions used in these experiments.

5. Summary and conclusions

1- Two different heat treatments were used to achieve martensitic α′ and lamellar α+β initial microstructures in a Ti-6Al-4V alloy and these materials were processed by high-pressure torsion (HPT) through 10 turns at room temperature. The results show that after HPT the hardness of the α′ alloy is higher than the α+β alloy (Hv ≈ 390 and ~350, respectively) and the grain size is smaller (~30 and ~40 nm, respectively). There are phase transformations of α′→α′+*fcc* and *α+β*→α during HPT in the martensitic and lamellar alloys, respectively

2- Following HPT, the samples were subjected to post-deformation annealing (PDA) for 60 min at temperatures in the range of 473 to 1023 K. The results show there are phase transformations of α′+*fcc*→*α+β+fcc* and α→*α+β* due to PDA up to 1023 K in the martensitic and lamellar alloys, respectively.

3- The initial martensitic microstructure leads to greater grain refinement during HPT with average grain sizes that are smaller after PDA. There is an *fcc* phase in the martensitic alloy after PDA and this appears to improve the strength.

4- An optimum very high yield strength (~1120 MPa) and ultimate tensile strength (~1200 MPa), combined with significant ductility (elongation to failure of ~26%), was achieved in the alloy processed by a combination of HPT in the martensitic state and PDA at 873 K for 60 min.

Acknowledgement

This work was supported by the European Research Council under Grant Agreement No. 267464-SPDMETALS.

References

1- S.L. Semiatin, V. Seetharaman, I. Weiss, Hot working of titanium alloys- an overview, Advances in the science and technology of titanium alloys processing, eds. I. Weiss, R. Srinivasan, P.J. Bania, D. Eylon, S.L. Semiatin, Warrendale, PA: TMS (1997) pp. 3-73.

2- I. Gurrappa, Characterization of titanium alloy Ti-6Al-4V for chemical, marine and industrial applications, Mater. Character. 51 (2003) 131-139.

3- M. Geetha, A.K. Singh, R. Asokamani, A.K. Gogia, Ti based biomaterials, the ultimate choice for orthopaedic implants – A review, Prog. Mater. Sci. 54 (2009) 397-425.

4- L.E. Murr, S.A. Quinones, S.M. Gaytan, M.I. Lopez, A. Rodela, E.Y. Martinez, D.H. Hernandoz, E. Martinez, F. Medina, R.B. Wicker, Microstructure and mechanical behavior of Ti-6Al-4V produced by rapid-layer manufacturing for biomedical applications, J. Mech. Behav. Biomed. Mater. 2 (2009) 20-37.

5- M.J. Donachie, Titanium, A Technical Guide, Metals Park, OH: ASM, 1988, pp. 57-74.

6- I.J. Polmear, Light Alloys, Metallurgy of the Light Alloys, Metals Park, OH: ASM 1984.

7- B.K. Damkroger, G.R. Edwards, Continuous cooling transformation kinetics in alpha-beta titanium alloys, Simulation and theory of evolving microstructure, ed. M.P. Anderson, Warrendale, PA: TMS (1990) pp. 129-150.

8- F.J. Gil, J.A. Planell, Growth order and activation energies for grain growth of Ti-6Al-4V alloy in β phase, Scr. Metall. Mater. 25 (1991) 2843-2848.

9- Y.T. Lee, M. Peters, G. Welsch, Elastic-moduli and tensile and physical-properties of heat-treated and quenched powder metallurgical Ti-6Al-4V-Alloy, Metall. Mater. Trans. A 22A (1991) 709-714.

10- R.Z. Valiev, R.K. Islamgaliev, I.V. Alexandrov, Bulk nanostructured materials from severe plastic deformation, Prog. Mater. Sci. 45 (2000) 103-189.

11- T.G. Langdon, Twenty-five years of ultrafine-grained materials: Achieving exceptional properties through grain refinement, Acta Mater. 61 (2013) 7035-7059.

12- A.P. Zhilyaev, S. Lee, G.V. Nurislamova, R.Z. Valiev, T.G. Langdon, Microstructure and microhardness evolution in pure nickel during high-pressure torsion, Scr. Mater. 44 (2001) 2753-2758.

13- A.P. Zhilyaev, G.V. Nurislamova, B.K. Kim, M.D. Baró. J.A. Szpunar, T.G. Langdon, Experimental parameters influencing grain refinement and microstructural evolution during high-pressure torsion, Acta Mater. 51 (2003) 753-765.

14- J. Wongsa-Ngam, M. Kawasaki, T.G. Langdon, A comparison of microstructures and mechanical properties in a Cu-Zr alloy processed using different SPD techniques, J. Mater. Sci. 48 (2013) 4653-4660.

15- A.P. Zhilyaev, T.G. Langdon, Using high-pressure torsion for metal processing: Fundamentals and applications, Prog. Mater. Sci. 53 (2008) 893-979.

16- R.Z. Valiev, Materials science: Nanomaterial advantage, Nature 419 (2002) 887-889.

17- C.C. Koch, Optimization of strength and ductility in nanocrystalline and ultrafine grained metals, Scr. Mater. 49 (2003) 657-662.

18- R.Z. Valiev, Nanostructuring of metals by severe plastic deformation for advanced properties, Nat. Mater. 3 (2004) 511-516.

19- R.Z. Valiev, A.V. Sergueeva, A.K. Mukherjee, The effect of annealing on tensile deformation behaviour of nanostructured SPD titanium, Scr. Mater. 49 (2003) 669-674.

20- O. Andreau, J. Gibicza, N.X. Zhang, Y. Huang, P. Jenei, T.G. Langdon, Effect of short-term annealing on the microstructures and flow properties of an Al-1% Mg alloy processed by high-pressure torsion, Mater. Sci. Eng. A 615 (2014) 231-239.

21- N. Maury. N.X. Zhang, Y. Huang, A.P. Zhilyaev, T.G. Langdon, A critical examination of pure tantalum processed by high-pressure torsion, Mater. Sci. Eng. A 638 (2015) 174-182.

22- H. Shahmir, J. He, Z. Lu, M. Kawasaki, T.G. Langdon, Effect of annealing on mechanical properties of a nanocrystalline CoCrFeNiMn high-entropy alloy processed by high-pressure torsion, Mater. Sci. Eng. A 676 (2016) 294-303.

23- A.V. Sergueeva, V.V. Stolyarov, R.Z. Valiev, A.K. Mukherjee, Enhanced superplasticiy in a Ti-6Al-4V alloy processed by severe plastic deformation, Scr. Mater. 43 (2000) 819-824.

24- R.S. Mishra, V.V. Stolyarov, C. Echer, R.Z. Valiev, A.K. Mukherjee, Mechanical behavior and superplasticity of a severe plastic deformation processed nanocrystalline Ti-6Al-4V alloy, Mater. Sci. Eng. A 298 (2001) 44-50.

25- A.V. Sergueeva, V.V. Stolyarov, R.Z. Valiev, A.K. Mukherjee, Superplastic behaviour of ultrafine-grained Ti-6A1-4V alloys, Mater. Sci. Eng. A 323 (2002) 318-325.

26- Y.C. Wang, T.G. Langdon, Influence of phase volume fractions on the processing of a Ti-6Al-4V alloy by high-pressure torsion, Mater. Sci. Eng. A 559 (2013) 861-867.

27- Y.C. Wang, T.G. Langdon, Effect of heat treatment on microstructure and microhardness evolution in a Ti-6Al-4V alloy processed by high-presure torsion, J. Mater. Sci. 48 (2013) 4646-4652.

28- J. Fu, H. Ding, Y. Huang, W. Zhang, T.G. Langdon, Influence of phase volume fraction on the grain refining of a Ti-6Al-4V alloy by high-pressure torsion, J. Mater. Res. Technol. 4(1) (2015) 2-7.

29- Z.Y. Hu, X.W. Cheng, Z.H. Zhang, H. Wang, S.L. Li, G.F. Korznikova, D.V. Gunderov, F.C. Wang, The influence of defect structures on the mechanical properties of Ti-6Al-4V alloys deformed by high-pressure torsion at ambient temperature, Mater. Sci. Eng. A 684 (2017) 1-13.

30- R.B. Figueiredo, P.R. Cetlin, T.G. Langdon, Using finite element modeling to examine the flow processes in quasi-constrained high-pressure torsion, Mater. Sci. Eng. A 528 (2011) 8198-8204.

31- J. Wang J, Z. Horita, M. Furukawa, M. Nemoto, N.K. Tsenev, R.Z. Valiev, Y. Ma, T.G. Langdon, An investigation of ductility and microstructural evolution in an Al-3% Mg alloy with submicron grain size, J. Mater. Res. 8 (1993) 2810-2818.

32- M. Furukawa, Z. Horita, M. Nemoto, R.Z. Valiev, T.G. Langdon, Microhardness measurements and the Hall-Petch relationship in an Al-Mg alloy with submicrometer grain size, Acta Mater. 44 (1996) 4619-4629.

33- Z. Horita, D.J. Smith, M. Furukawa, M. Nemoto, R.Z. Valiev, T.G. Langdon, An investigation of grain boundaries in submicrometer-grained Al-Mg solid solution alloys using high-resolution electron microscopy, J. Mater. Res. 11 (1996) 1880-1890.

34- Z. Horita, D.J. Smith, M. Nemoto, R.Z. Valiev, T.G. Langdon, Observations of grain boundary structure in submicrometer-grained Cu and Ni using high-resolution electron microscopy, J. Mater. Res. 13 (1998) 446-450.

35- Y.T. Lee, M. Peters, G. Welsch, Elastic-moduli and tensile and physical-properties of heat-treated and quenched powder metallurgical Ti-6Al-4V-Alloy, Metall. Mater. Trans. A 22A (1999) 709-714.

36- B.D. Cullity, S.R. Stock, Elements of X-ray Diffraction. 3rd ed, Englewood Cliffs, NJ: Prentice Hall 2001.

37- A.V. Sergueeva, V.V. Stolyarov, R.Z. Valiev, A.K. Mukherjee, Enhanced superplasticity in a Ti-6Al-4V alloy processed by severe plastic deformation, Scripta Mater. 43 (2000) 819-824.

38- F.J. Gil, J.M. Manero, J.A. Planell, Decomposition of α′ martensite plates of Ti-6Al-4V alloy at different annealing temperatures and heat treatment times, ed. P.A. Blenkinsop, W.J. Evans, H.M. Flower, Titanium’95: Science and Technology, The Institute of Materials, London, UK (1996) pp. 2454-2461.

39- D.H. Shin, I. Kim, J. Kim, Y.T. Zhu, Shear strain accommodation during severe plastic deformation of titanium using equal channel angular pressing, Mater. Sci, Eng. A 334 (2002) 239-245.

40- D.H. Shin, I. Kim, J. Kim, Y.S. Kim, S.L. Semiatin, Microstructure development during equal-channel angular pressing of titanium, Acta Mater. 51 (2003) 983-996.

41-P. Castany, F. Pettinari-Sturmel, J. Douin, A. Coujou, In situ transmission electron microscopy deformation of the titanium alloy Ti-6Al-4V: Interface behaviour, Mater. Sci. Eng. A 483-484 (2008) 719-722.

42- S.V. Zherebtsov, G.S. Dyakonov, A.A. Salem, S.P. Malysheva, G.A. Salishchev, S.L. Semiatin, Evolution of grain and subgrain structure during cold rolling of commercial-purity titanium, Mater. Sci. Eng. A 528 (2011) 3474-3479.

43- H. Shahmir, T.G. Langdon, An evaluation of the hexagonal close-packed to face-centered cubic phas transforemation in a Ti-6Al-4V alloy during high-pressure torsion, Mater. Sci. Eng. A 704 (2017) 212-217.

44- F.X. Gil Mur, D. Rodríguez, J.A. Planell, Influence of tempering temperature and time on the α′-Ti-6A1-4V martensite, J. Alloy. Compounds 234 (1996) 287-289.

45- R. Jing, C.Y. Liu, M.Z. Ma, R.P. Liu, Microstructural evolution and formation mechanism of FCC titanium during heat treatment processing, J. Alloy. Compounds 552 (2013) 202-207.

46- D.H. Hong, T.W. Lee, S.H. Lim, W.Y. Kim, S.K. Hwang, Stress-induced hexagonal close-packed to face-centered cubic phase transformation in commercial-purity titanium under cryogenic plane-strain compression, Scr. Mater. 69 (2013) 405-408.

47- Y.H. Zhao, Y.Z. Guo, Q. Wei, A.M. Dangelewicz, C. Xu, Y.T. Zhu, T.G. Langdon, Y.Z. Zhou, E.J. Lavernia, Influence of specimen dimensions on the tensile behavior of ultrafine-grained Cu, Scr. Mater. 59 (2008) 627-630.

48- Y.H. Zhao, Y.Z. Guo, Q. Wei, T.D. Topping, A.M. Dangelewicz, Y.T. Zhu, T.G. Langdon, E.J. Lavernia, Influence of specimen dimensions and strain measurement methods on tensile stress-strain curves, Mater. Sci. Eng. A 525 (2009) 68-77.

49- P.H.R. Pereira, Y.Huang, M. Kawasaki, T.G. Langdon, An examination of the superplastic characteristics in Al-Mg-Sc alloys after processing, J. Mater. Res. (2017) DOI: 10.1557/jmr.2017.286.

50- A.V. Sergueeva, J. Zhou, B.E. Meacham, D.J. Branagan, Gage length and sample size effect on measured properties during tensile testing, Mater. Sci. Eng. A 526 (2009) 79-83.

Table caption

Table 1 Microhardness, YS, UTS and elongation (δ) of α′ and α+β-Ti-6Al-4V alloys in the initial condition and after PDA at 873-1023 K for 60 min.

Figures captions

Fig. 1 Optical micrographs of the Ti-6Al-4V microstructures after (a) annealing at 1273 K for 30 min followed by water quenching (α′ alloy) and (b) annealing at 1023 K for 45 min followed by air quenching and then annealing at 873 K for 3 h followed by furnace quenching (α+β alloy).

Fig. 2 TEM images and corresponding SAED patterns of (a) α′ and (b) α+β alloys after HPT processing through 10 turns.

Fig. 3 (a) High magnification TEM image and corresponding SAED pattern of nanocrystalline α′ alloy: the diffraction pattern shows a series of *hcp* and *fcc* phases; (b) dark-field image relating to the diffraction spot (*fcc* phase) surrounded by a white circle in Fig. 3(a).

Fig. 4 Dependence of Vickers microhardness of the HPT-processed samples for the α′ and α+β alloys on the annealing temperature using annealing times of 60 min: the lower dashed lines denote the Vickers microhardness for the initial α′ and α+β alloys.

Fig. 5 Stress-strain curves at an initial strain rate of 1.0×10^{-3} s^{-1} after HPT followed by PDA at different temperatures for (a) α′ and (b) α+β alloys: the stress-strain curves for the α′ and α+β alloys in the initial conditions are also shown by the dashed curves.

Fig. 6 X-ray patterns of (a) α′ and (b) α+β alloys before and after HPT processing through 10 turns and after PDA at 773, 873 and 973 K for 60 min.

Fig. 7 SEM images of (a-c, left column) α′ and (d-f, right column) α+β alloys after PDA at temperatures from 923 to 1023 K for 60 min.

***Figure(s)**

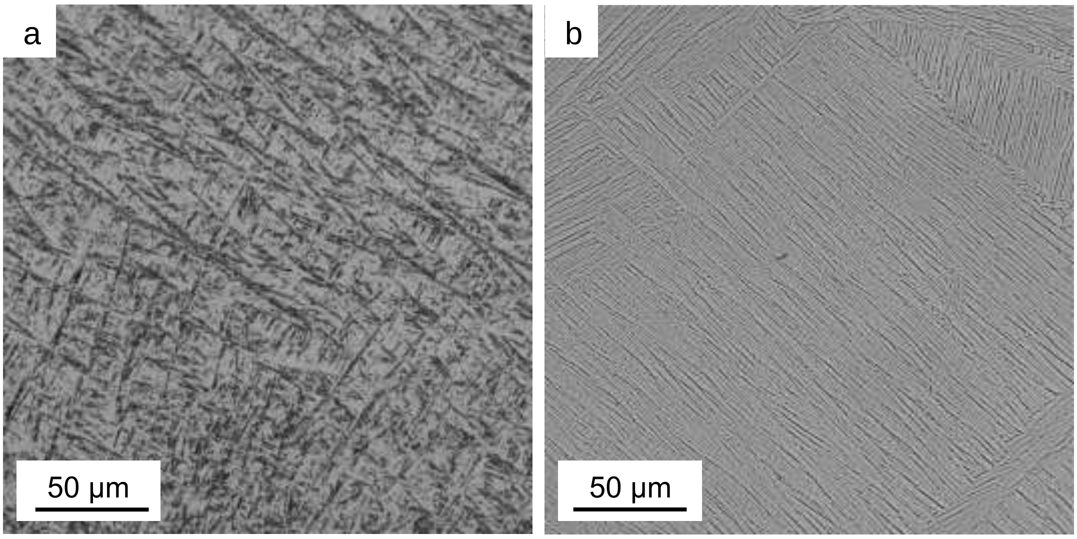

Fig. 1 Optical micrographs of the Ti-6Al-4V microstructures after (a) annealing at 1273 K for 30 min followed by water quenching (α′ alloy) and (b) annealing at 1023 K for 45 min followed by air quenching and then annealing at 873 K for 3 h followed by furnace quenching (α+β alloy).

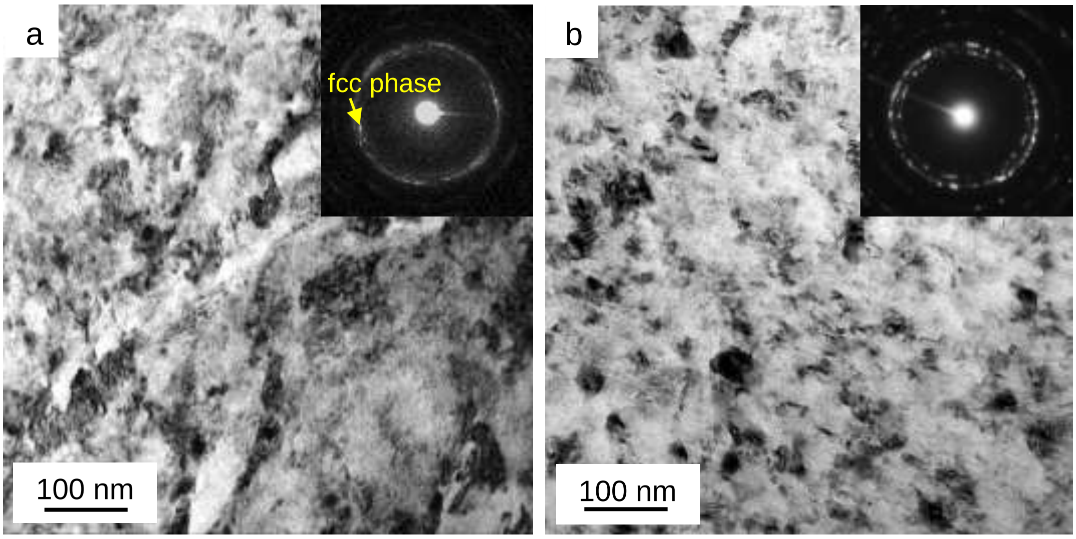

Fig. 2 TEM images and corresponding SAED patterns of (a) α′ and (b) α+β alloys after HPT processing through 10 turns.

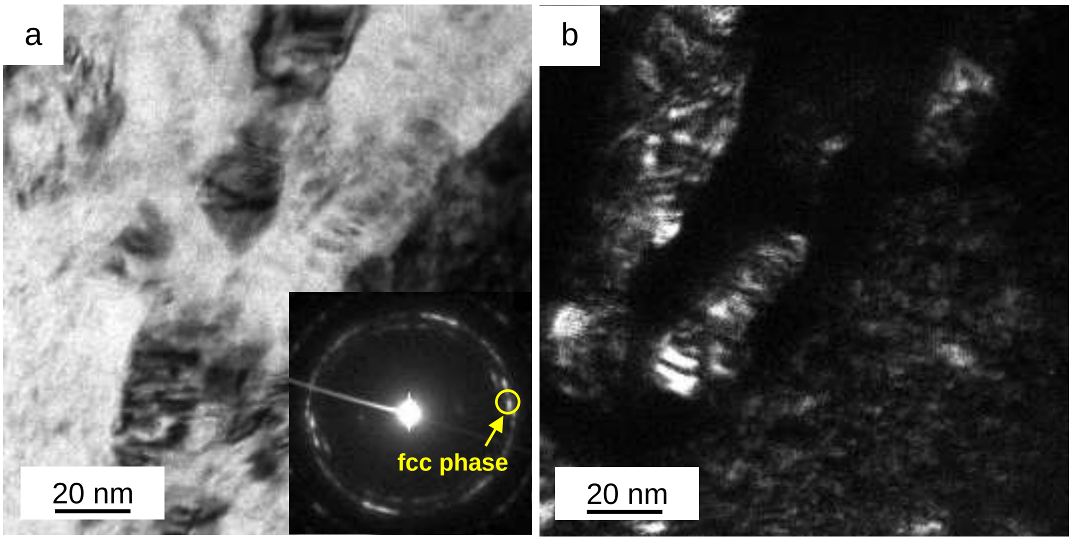

Fig. 3 (a) High magnification TEM image and corresponding SAED pattern of nanocrystalline α′ alloy. The diffraction pattern shows a different series of *hcp* and *fcc* phases. (b) The dark-field image relates to the diffraction spot (*fcc* phase) surrounded by a white circle.

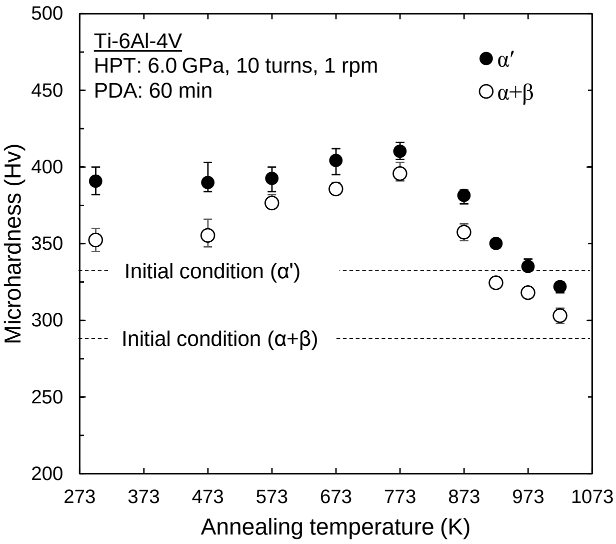

Fig. 4 Dependence of Vickers microhardness of the HPT-processed samples for the α′ and α+β alloys on the annealing temperature using annealing times of 60 min: the lower dashed lines denote the Vickers microhardness for the initial α′ and α+β alloys.

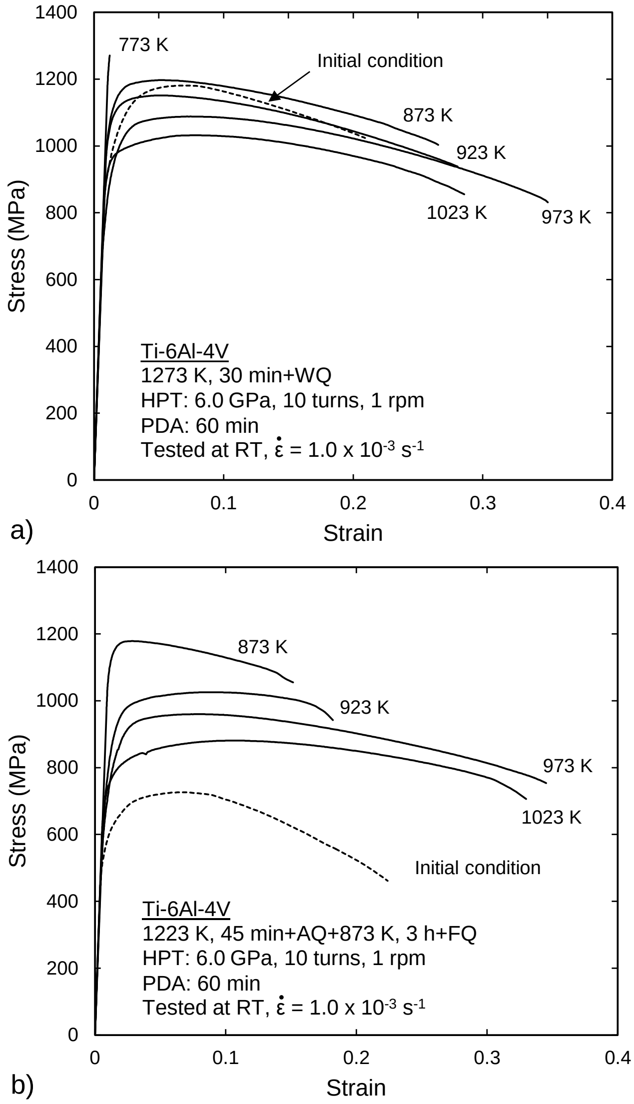

Fig. 5 Stress-strain curves at an initial strain rate of 1.0×10^{-3} s^{-1} after HPT followed by PDA at different temperatures for (a) α′ and (b) α+β alloys: the stress-strain curves for the α′ and α+β alloys in the initial conditions are also shown by the dashed curves.

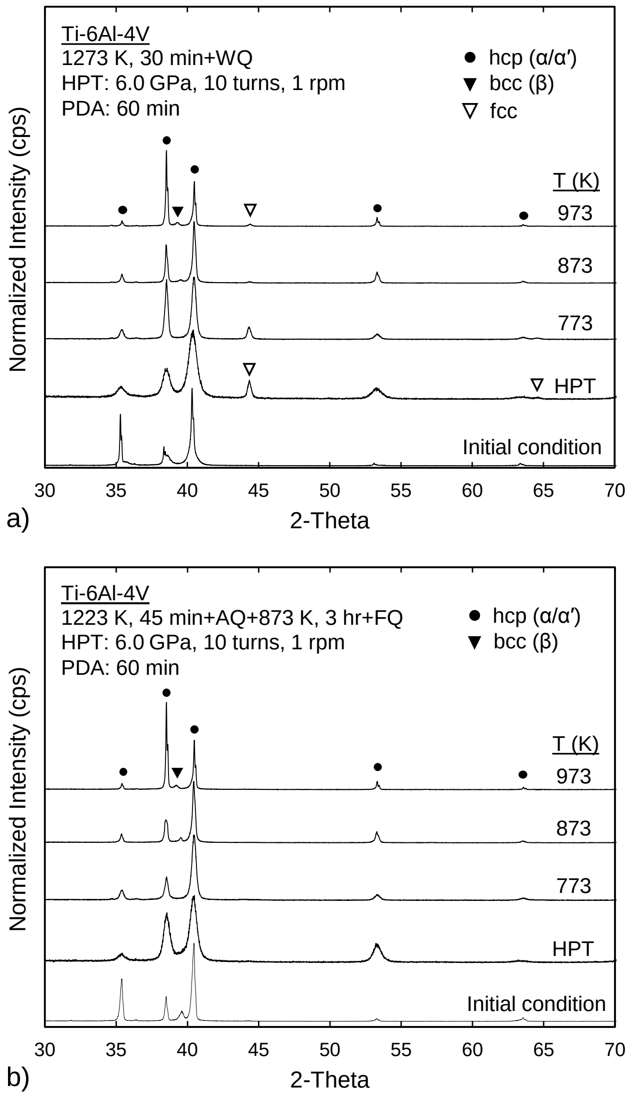

Fig. 6 X-ray patterns of (a) α′ and (b) α+β alloys before and after HPT processing through 10 turns and after PDA at 773, 873 and 973 K for 60 min.

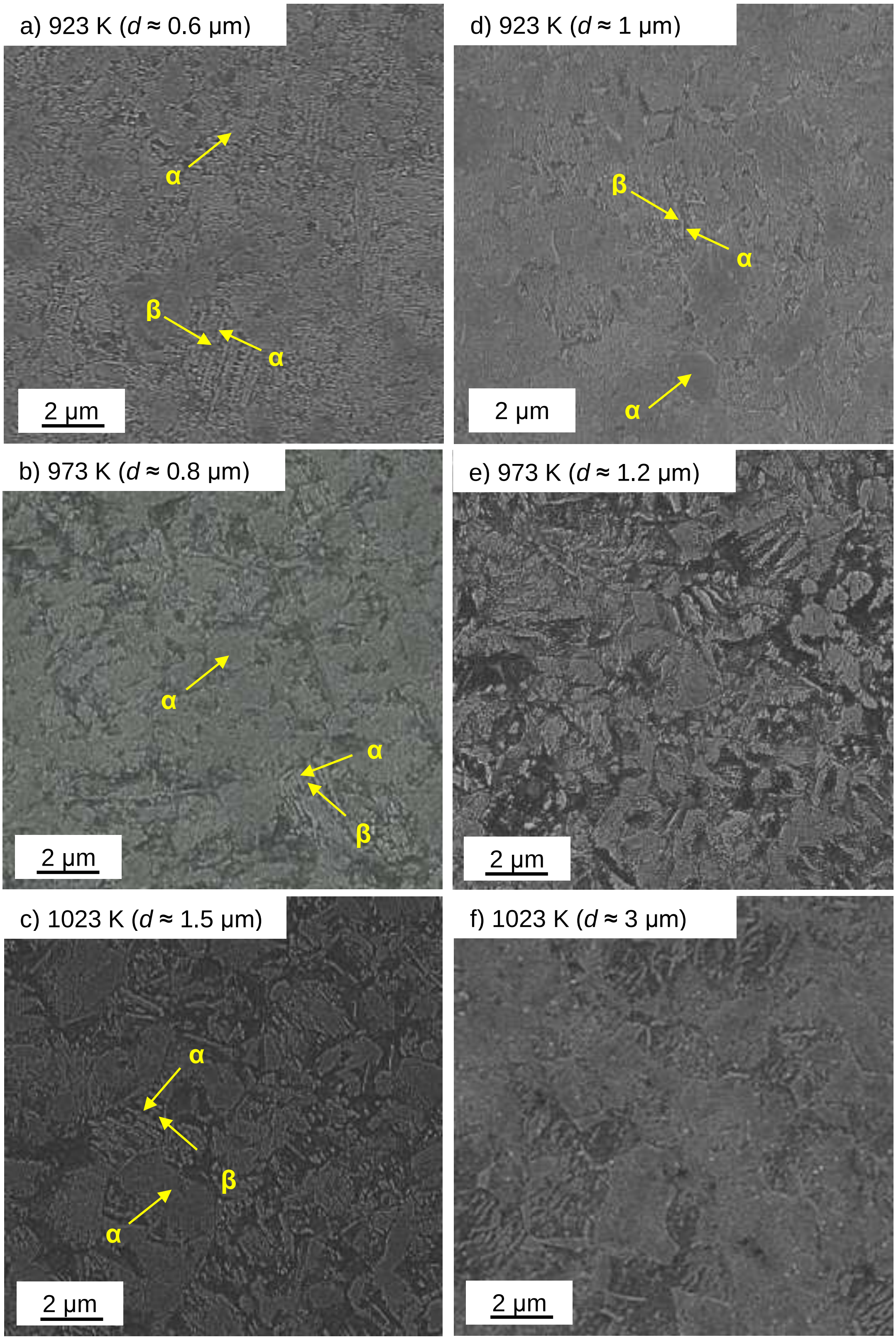

Fig. 7 SEM images of (a-c, left column) α′ and (d-f, right column) α+β alloys after PDA at temperatures from 923 to 1023 K for 60 min.

Table(s)

Table 1. Microhardness, YS, UTS and elongation (δ) of α′ and α+β-Ti-6Al-4V alloys in initial condition and after PDA at 873-1023 K for 60 min.

Alloy	Annealing temperature (K)	Hv	YS (MPa)	UTS (MPa)	δ (%)
α'	Initial condition	330 ± 3	930 ± 32	1190 ± 25	20 ± 3
	873	380 ± 4	1120 ± 40	1200 ±28	26 ± 2
	923	350 ± 2	1050 ± 25	1150 ± 10	28 ± 2
	973	335 ± 3	920 ± 30	1080 ± 22	35 ± 3
	1023	320 ± 3	810 ± 25	1030 ± 15	28 ± 4
α+β	Initial condition	290 ± 4	250 ± 38	730 ± 30	23 ± 4
	873	360 ± 4	1100 ± 30	1180 ± 20	15 ± 2
	923	325 ± 3	750 ± 25	1025 ± 12	18 ± 5
	973	320 ± 3	740 ± 35	960 ± 24	34 ± 3
	1023	300 ± 4	660 ± 22	880 ± 10	33 ± 2